Journal of Applied Polymer Science

High Electrical Conductivity of Nylon 6 Composites Obtained with Hybrid Multiwalled Carbon Nanotube/Carbon Fiber Fillers

Xiang-Dong Zhu, Chong-Guang Zang, Qing-Jie Jiao
State Key Laboratory of Explosive Science and Technology, Beijing Institute of Technology, Beijing 100081, People's Republic of China
Correspondence to: C.-G. Zang (E-mail: zangchongguang@bit.edu.cn)

ABSTRACT: The synergetic effect of multiwalled carbon nanotubes (MWNTs) and carbon fibers (CFs) in enhancing the electrical conductivity of nylon 6 (PA6) composites was investigated. To improve the compatibility between the fillers and the PA6 resin, we grafted γ-aminopropyltriethoxy silane (KH-550) onto the MWNTs and CFs after carboxyl groups were generated on their surface by chemical oxidation with nitric acid. Fourier transform infrared spectroscopy and thermogravimetric analysis proved that the KH-550 molecules were successfully grafted onto the surface of the MWNTs and CFs. Scanning electron microscopy and optical microscopy showed that the obtained modified fillers reduced the aggregation of fillers and resulted in better dispersion and interfacial compatibility. We found that the electrical percolation threshold of the MWNT/PA6 and CF/PA6 composites occurred when the volume fraction of the fillers were 4 and 5%, respectively. The MWNT/CF hybrid-filler system exhibited a remarkable synergetic effect on the electrically conductive networks. The MWNT/7% CF hybrid-filler system appeared to show a second percolation when the MWNT volume fraction was above 4% and a volume resistivity reduction of two orders of magnitude compared with the MWNT/PA6 system. The mechanical properties of different types of PA6 composites with variation in the filler volume content were also studied. © 2014 Wiley Periodicals, Inc. J. Appl. Polym. Sci. **2014**, *131*, 40923.

KEYWORDS: composites; fibers; grafting; graphene and fullerenes; nanotubes

Received 20 November 2013; accepted 25 April 2014
DOI: 10.1002/app.40923

INTRODUCTION

In comparison with a single-filler composite system, systems with more fillers take advantage of two or more different dimension filler particles to endow some special performance on polymer composites, such as their mechanical properties,[1–5] heat-conducting properties,[6–10] and electrical conductivity (σ);[11–16] they have been paid much attention because they possess the characteristics of each filler. Polymer composite materials with different fillers, including carbon fibers (CFs), glass fibers, inorganic particles, metal powder, nanoparticles, and nanotubes, have been reported, where filler particles with different dimensions in terms of fibers, platelets, and granules in micrometer order and nanoscale size have been formed. Among these fillers, carbon nanotubes and CFs have attracted a great deal of interest because of their excellent electrical and mechanical properties. In particular, both of them can easily comprise a conductive network in the polymer matrix; this is very valuable for the enhancement of the conductivity of the polymer matrix.[8,16]

Multiwalled carbon nanotubes (MWNTs) composed of nanoscale multiple tubes of graphite layers are considered to be perfect candidates as conductive fillers in polymers, and they are expected to lead to high mechanical and electrical properties.[17] However, their performance is often less than expected because of the large surface areas and poor interfacial bonding strength with the polymer matrix and because the excellent properties of the MWNTs cannot produce the best possible results.[18,19] Therefore, to increase the interfacial compatibility between the MWNTs and the matrix, the chemical functionalization of the surface has been used to reduce aggregations.[20–24]

CFs are one of the most promising conductive micrometer-sized fillers exhibiting excellent mechanical properties and electrical and thermal conductivities.[25] Lonjon et al.[15] reported that the addition of CFs significantly improved the conductivity of MWNT/polymer composites. The polymers adhered poorly to the surface as a result of the insert and smooth surface of the CFs. A similar modification process was used to modify the surface of the CFs as MWNTs in this study. With a hybrid-filler system of MWNTs and CFs, two kinds of usage modes could be formed. On the one hand, a covalent bond connection to form a three-dimensional (3D) filler was achieved by a functional group reaction,[26] or the MWNTs could be directly grown on the CF surface.[27] On the other hand, the conductive network

depended mainly on the connection conductivity among the two differently sized particles and the polymer matrix. The second method could be divided into two cases according to the different lengths and uses of the CFs. One was the addition of long CFs into composite materials composed of the MWNTs and the polymer.[15] The other method was the simultaneous addition of short carbon fibers (SCFs) and MWNTs to the polymer matrix; to the best of our knowledge, this has not been reported in the literature.

In this study, melt blending was used to combine nanoscale MWNTs and micrometer-order SCFs to improve the σ of nylon 6 (PA6). The MWNTs and CFs were surface-treated by chemical oxidation and treated with the coupling agent γ-aminopropyltriethoxy silane (KH-550); this provided deep insight to the roles of the interfacial interaction in the fillers and resin. A remarkable synergetic effect was demonstrated in the 3D MWNT/CF hybrid-filler system; this effectively enhanced σ of the PA6 composites. In this study, we also investigated the effects of the functionalized fillers on the mechanical properties of the PA6 composites.

EXPERIMENTAL

Materials

PA6 pellets (CM1017) were obtained commercially from Toray (Japan) in this experiment. MWNTs were produced by Shenzhen Nanotech Port Co., Ltd. (People's Republic of China; model S-MWNTs-1030, outer diameter = 10–30 nm, length = 10–50 μm, purity > 95%, special surface area = 40–300m^2/g). The CFs were produced by Liaoning Anke Carbon Fibre Co. (model 12K-SCF, resistivity = 1.6Ω·cm, diameter = 6.5 μm, length = 3 mm). KH-550 was purchased from Anhui Tianchang Greenness Chemical Plant.

Instrumental Analysis

The functional groups of the prepared samples were detected by Fourier transform infrared (FTIR) spectroscopy via an IFS 66V/S FTIR spectrometer (Bruker, Germany) with the KBr pellet method in the range 750–4000 cm^{-1}. Thermogravimetric analysis (TGA) was achieved by a Netzsch TG209F1 thermogravimetric analyzer at a heating rate of 20°C/min under a nitrogen atmosphere from ambient temperature to 800°C. Morphological analysis of PA6 composites was done by cold field emission scanning electron microscopy (SEM; S-4800, Hitachi High-Technologies Corp.). The fractured surfaces were gold plated and then mounted over an aluminum stub with double-sided electric adhesive tape. The vacuum was on the order of 10^{-4} to 10^{-6} mmHg during the scanning of the composite specimens. The dispersion of the fillers in the matrix was observed with an XP-203 optical microscope (Changfang Optical Instrument Co., Shanghai, China) with a CANY-V1.0 microscopic imaging system. The samples were hot-pressed and compressed into films with a thickness of about 50–80 μm.

The tensile properties tests were performed on the basis of an ASTM procedure with a model CMT4104 electromechanical universal testing machine. The specimen dimensions were 119 × 5.8 × 3.9 mm^3.

The direct-current (dc) bulk electrical resistivity (ρ; Ω·cm) of the conducting composites was measured by a four-contact scheme with an EST 991 electric and electrostatic shielding materials volume resistivity measure instrument. Every data point was tested three times, and the average value was calculated. A constant current was passed with a dc voltage source. ρ was calculated by Ohm law:

$$\rho = \frac{Vwh}{Il} \quad (1)$$

where V is the voltage; I is the current; w and h is the width and height of the specimens, respectively; and l is the distance between inside metal electrodes. In this study, the parameters l, w, and h of the specimens were 20, 10, and 2 mm, respectively. All of the measurements were done at room temperature. Before measurement, all of the samples were kept *in vacuo* at 60°C for 24 h.

Experimental Procedure

To achieve KH-550 grafted onto the surface of the MWNTs, the MWNTs were functionalized via an oxidation method to effectively generate carboxyl groups on their surface in advance. First, the MWNTs were treated with 69% HNO_3 with an ultrasonic bath at 80°C for 8 h. After that, the MWNTs were infused with 0.1 mol/L HCl for 30 min, then filtered by deionized (DI) water until the pH value reached 7, and dried by a drier at 100°C for 8 h. The resulting oxidized MWNTs were defined as O-MWNTs.

To effectively generate carboxyl groups on the surface of the CFs, first, it was oxidized in a muffle oven at 420°C for 1 h to remove the epoxy resin layer on its surface and then washed and filtered with ethanol. Subsequently, CFs were ultrasonic treated with 69% HNO_3 at 60°C for 4 h. The resulting oxidized CFs were defined as O-CFs.

A concentration of 1 wt % KH-550 was dissolved into 200 mL of an acetone solution (a mixture of acetone and DI water with a volume ratio of 5:1) to obtain a KH-550 acetone solution, and then, O-MWNTs were added to the solution. Then, the solution was ultrasonically treated to uniformly disperse the O-MWNTs into the KH-550 acetone solution until the acetone volatilized completely into the air. The KH-550 handling process of O-CFs was similar to that of the O-MWNTs. The KH-550 modified products were washed three times with DI water dried at 70°C for 6 h in a vacuum-drying oven. The overall synthetic pathway is shown in Figure 1.

Specimen Preparation

PA6 composites containing different kinds of MWNTs and different CF contents were prepared via a melt-compounding method with a twin-screw mixer at 250°C for 10 min with a screw speed of 100 rpm. The melt-mixed PA6 composites were compression-molded at 250°C under a pressure of 150 bar and allowed to cool at room temperature to obtain the composite samples.

RESULTS AND DISCUSSIONS

Characteristics of the MWNTs and CFs

The existence of KH-550 functionalities on the MWNT and CF surface were confirmed by FTIR spectroscopy. Figure 2 shows the typical FTIR spectrum obtained for the pristine MWNTs,

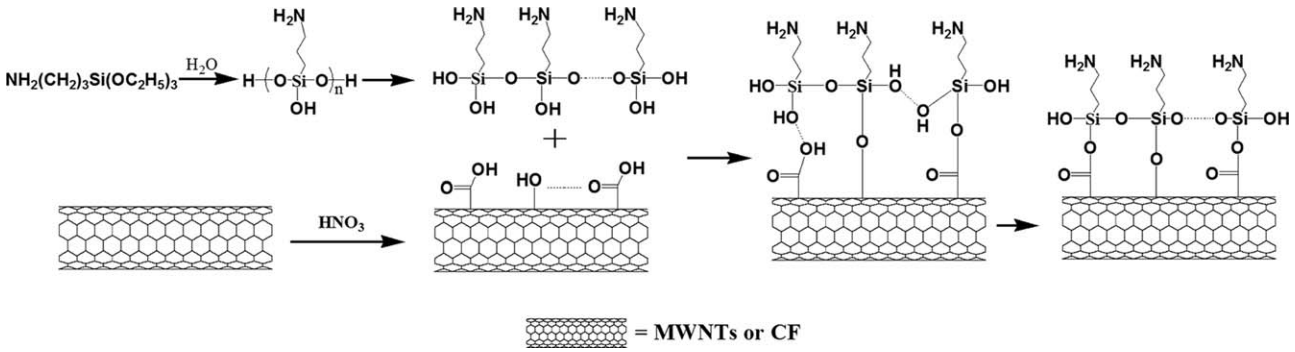

Figure 1. Synthetic pathway of the KH-550 coupled reaction.

acid MWNTs, KH-550-treated MWNTs, pristine CFs, acid CFs, and KH-550-treated CFs. The bands in all of the samples around 2955 and 2840 cm^{-1} were attributed to the asymmetric (aCH_2) and symmetric (sCH_2) stretching mode of the C—H bond.[28] The peaks around 3430 and 1630 cm^{-1} of pristine and acid functional MWNTs and CFs, respectively, were due to the stretching mode of O—H and C=C, respectively.[29,30] In the acid functional MWNTs and CFs, the bands at 1720 and 1718 cm^{-1} were due to the C=O stretching of —COOH.[30] The bands at 1378 and 1380 cm^{-1} were assigned to the O—H vibrations of the C—OH groups, and the peak at 1050 cm^{-1} was due to the C—O stretching vibrations.[31] For the KH-550-treated MWNTs, the existence of a doublet at 3438/3380 cm^{-1} suggested the N—H stretching vibrations of C—NH_2, the scissoring vibrations of N—H appeared at 1570 cm^{-1}, and the peak of 1120 cm^{-1} corresponded to the C—N of the alkyl chains of the KH-550 moieties.[32] The doublet at 3438/3380 cm^{-1} of C—NH_2 of KH-550 exhibited a similar intensity. However, the weak peak at 3380 cm^{-1} may have been caused by the O—H stretching vibrations that covered it. Furthermore, typical signals at 1029 and 920 cm^{-1} demonstrated the Si—O—Si of the hydroxylation of the KH-550 molecules on the surface of the functional MWNTs.[33] The FTIR spectrum of the KH-550-coupled CFs showed a similar tendency compared with the functional MWNTs.

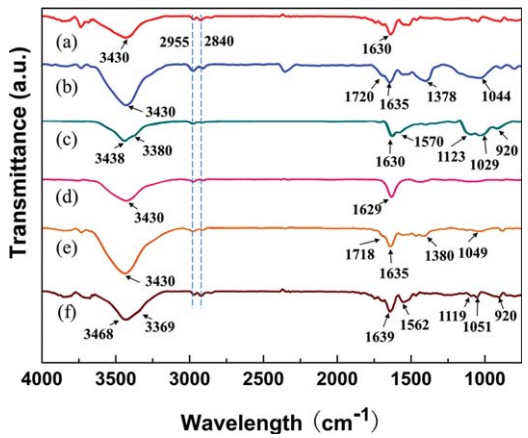

Figure 2. FTIR spectra corresponding to the (a) pristine MWNTs, (b) acid MWNTs, (c) KH-550-treated MWNTs, (d) pristine CFs, (e) acid CFs, and (f) KH-550-treated CFs. [Color figure can be viewed in the online issue, which is available at wileyonlinelibrary.com.]

The quality value of the functional groups was evaluated by TGA. Figure 3 shows the TGA curves of the pristine MWNTs and CFs compared with the KH-550-coupled MWNTs and CFs.

As observed from the TGA curve in Figure 3, no functional groups were detected in the raw MWNTs and CFs, and the weight losses of 0.9 and 0.5% in the raw materials were caused by amorphous carbon, moisture, metal particles, and volatile carbonaceous impurities. The TGA spectra of the KH-550-coupled MWNTs could be divided into three steps. The first step from room temperature to 150°C exhibited about a 2.4% weight loss corresponding to the volatile matter. The second step caused an approximately 4.9% weight loss; this was due to the unreacted oxygen-containing groups (—COOH, —OH) and physically deposited KH-550 molecules on the surface of the MWNTs from 150 to 380°C.[34] The last step from 380 to 800°C displayed the largest weight loss percentage (14.22%) as a result of the decomposition of KH-550, which attached through covalent bonding. The result further proved the successful grafting of KH-550 on the surface of the MWNTs through the coupling reaction. The TGA curve of the KH-550-functionalized CFs possessed a similar development tendency compared to that of the MWNTs. The distinction of the first and second steps was not obvious; this may have been due to little volatile matter on the surface of the CFs. The major weight loss in the third step of KH-550 on the CFs was calculated to be about 1.74%; the CFs were attached through covalent bonding.

The results of FTIR spectroscopy and TGA demonstrated that there existed many oxygen-containing and —NH_2 groups on the surface of the KH-550-coupling-treated MWNTs and CF. This benefited the dispersion of interfacial compatibility between the fillers and polymer matrix.

Morphological Analysis

Any inhomogeneity of the fillers could result in structural defects; this was closely related to the σ of the polymer composite. So, the morphologies of the fractured surfaces of different types of PA6 composites were investigated by SEM.[35–37] Figure 4 displays the SEM microphotographs of different types of MWNTs and the single-filler composite system. The raw MWNTs were observed to have a uniform diameter and a smooth surface, and the end of the tube was closed [Figure 4(a)]. As shown in Figure 4(b), the surface became rough after it was treated with KH-550; this indicated that the KH-550 molecule was successfully grafted onto the MWNTs. Figure

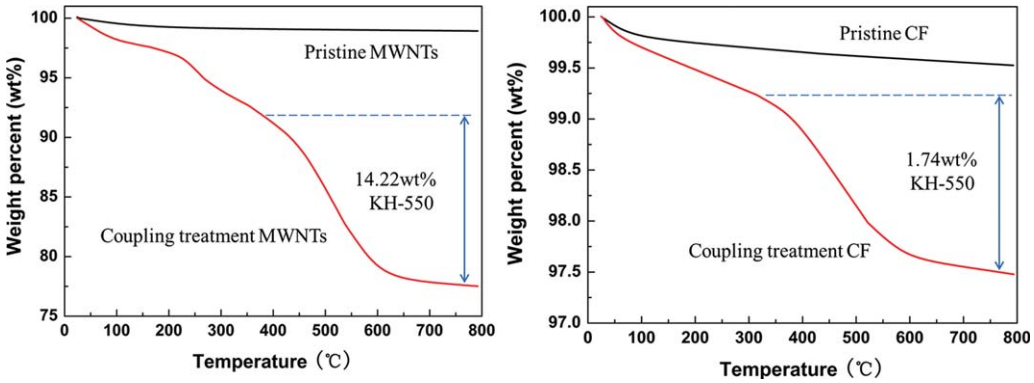

Figure 3. TGA spectra of the different types of MWNTs and CFs. [Color figure can be viewed in the online issue, which is available at wileyonlinelibrary.com.]

4(c,d) represents the cross-sectional morphology of the MWNT/PA6 composites [volume fraction of the multiwalled carbon nanotubes (φ_{MWNTs}) = 4%] before and after the MWNT coupling treatment with KH-550. As shown in Figure 4(c), there were many MWNT clusters in the PA6 matrix and even some MWNTs extracted from the matrix; this suggested that the original MWNTs were detrimental to their compatibility and that there was adhesion between the MWNTs and the matrix, although a lot of tubal MWNTs after the surface treatment with KH-550 were homogeneously dispersed in the PA6 matrix [Figure 4(d)]. This demonstrated that the coupling treatment process was effective for the MWNT dispersion and interfacial bonding in the PA6 matrix. Figure 5 shows the SEM images of the CF/PA6 composites [volume fraction of the carbon fibers (φ_{CF}) = 5%] with raw CFs and coupling-treated CFs with KH-550.

Figure 5(a) shows the image of the raw CF/PA6 composites with CFs falling off from the polymer matrix and the fracture surface. As shown in Figure 5(b), PA6 could hardly adhere to the surface of the raw CFs because of the smooth surface and poor adhesion. This demonstrated the bad interfacial compatibility between the raw CFs and PA6. In a comparison of Figure 5(a) with Figure 5(c), we observed that the bond between the CFs and the matrix in KH-550 was greater than that in the raw CF/PA6 composites. In addition, as shown in Figure 5(a), the raw CFs scattered parallel in the matrix, whereas the KH-550-treated CFs oriented in more than one direction and comprised a 3D network, as presented in Figure 5(c). Moreover, the surface of the coupling-treated CFs was adhered to a certain amount of the PA6 matrix [Figure 5(d)]. All of this proved that the coupling agent KH-550 contributed to the scattering of the CFs in the polymer and enhanced the interfacial bonding between the CFs and PA6.

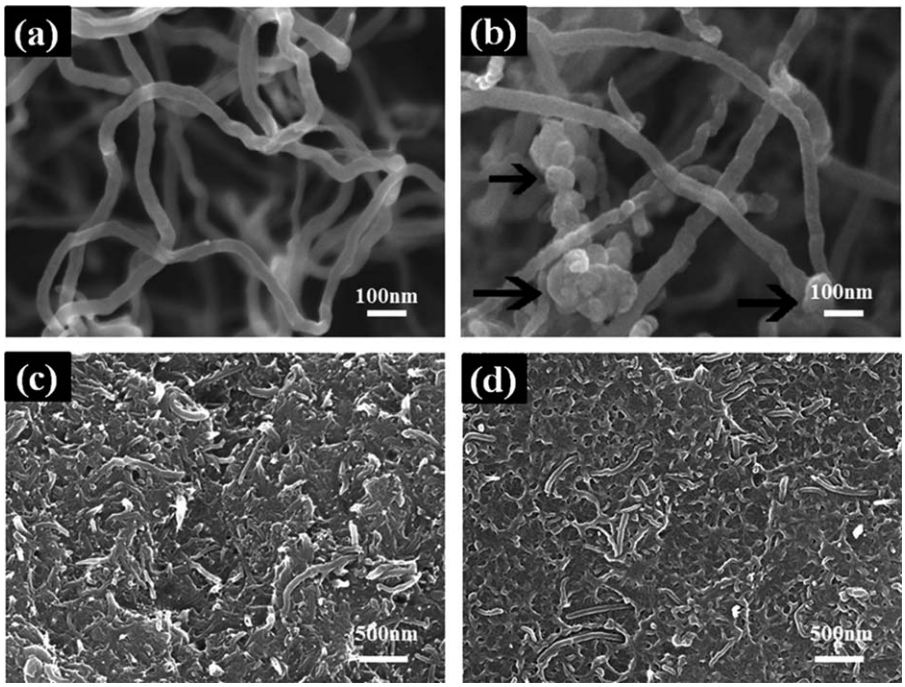

Figure 4. SEM images of the different types of the MWNTs and MWNT/PA6 composites (φ_{MWNTs} = 4%): (a,b) raw MWNTs and KH-550-treated MWNTs, respectively, and (c,d) raw MWNT/PA6 and KH-550-treated MWNT/PA6, respectively.

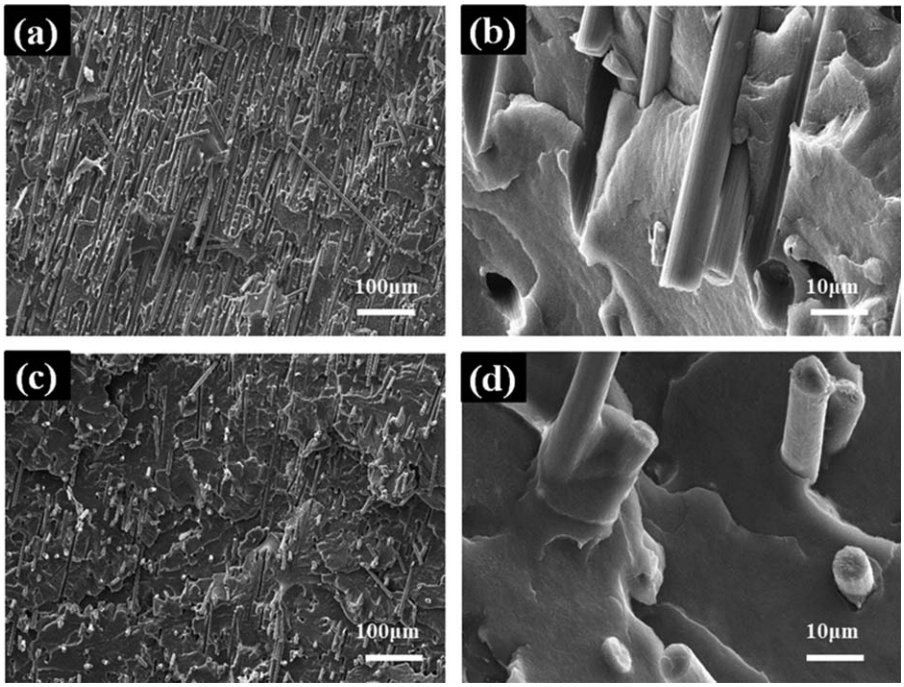

Figure 5. SEM images of the different types of CF/PA6 composites ($\varphi_{CF} = 5\%$): (a,b) raw CF/PA6 at lower and higher magnifications and (c,d) KH-550-treated CF/PA6 at lower and higher magnifications.

Figure 6 shows the SEM images of the MWNT/7% CF hybrid-filler system when φ_{MWNTs} was 4%. Compared with the single-filler system [Figure 5(c)], the CFs in the hybrid-filler-system polymer composites showed a more obvious 3D scattering in the matrix because the rigid MWNTs inhibited the further aggregation of the CFs [Figure 6(a)]. This allowed an electrically conductive network to form by the mutual contact of the CFs with each other. Figure 6(b) shows that the MWNTs were distributed in the gap of the conductive frame of the CFs; this demonstrated that the network of the hybrid filler of the MWNT/CF system had more electrically conductive channels than the single-filler system.

The optical microscopy showed the dispersion ability of the fillers in the PA6 composites,[38] as shown in Figure 7. Figure 7(a) shows some big agglomerations of MWNTs, and some area without MWNTs was found. This was due to the high degree of entanglement of the raw MWNTs and suggested the poor dispersion. However, the KH-550-treated MWNTs in the matrix showed that the size and amount of aggregations were much lower than those of raw MWNTs, as shown in Figure 7(b). The CF/PA6 composites possessed a similar state compared with the MWNTs. Obviously, the raw CFs in the polymer matrix scattered in a parallel manner, and some agglomerations were observed. This implied that the raw CFs were not effectively dispersed during melt blending [Figure 7(c)]. However, the coupling-treated CFs in the matrix oriented in more than one direction and comprised a 3D network [Figure 7(d)]; this was in agreement with earlier analysis in the SEM section. For the MWNT/7% CF/PA6 composite, the CFs exhibited the best state of dispersion and contact with each other to form a 3D structure. Furthermore, the MWNTs homogeneously dispersed in the gap of the main truss of the 3D network of the CFs [Figure 7(e,f)].

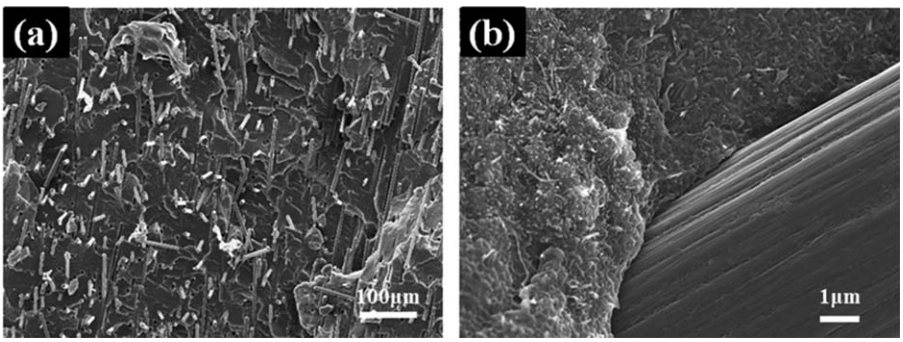

Figure 6. SEM images of the MWNT/7% CF/PA6 composites: (a) lower magnification and (b) higher magnification. The latter shows MWNTs close to the CFs in the PA6 composites.

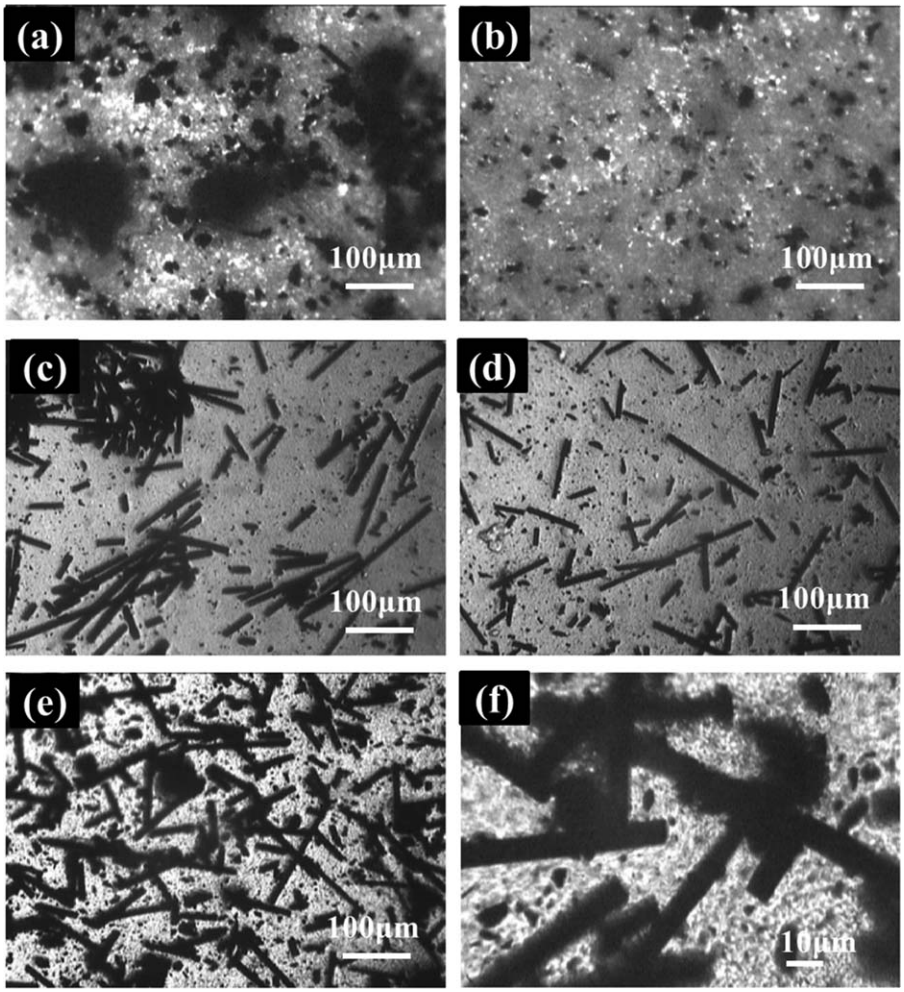

Figure 7. Optical microscopy images of the different types of composites: (a,b) raw MWNT/PA6 and KH-550-treated MWNT/PA6 composites, respectively; (c,d) raw CF/PA6 and KH-550-treated CF/PA6 composites, respectively; and (e,f) MWNT/7% CF/PA6 composites at lower and higher magnifications, respectively.

In conclusion, the hybrid-filler systems had the best dispersion in the polymer composites compared with the single-filler system.

Electrical Properties

Figure 8 presents the σ values of the MWNT/PA6 composites with uncoupled and coupling-treated MWNTs versus the filler

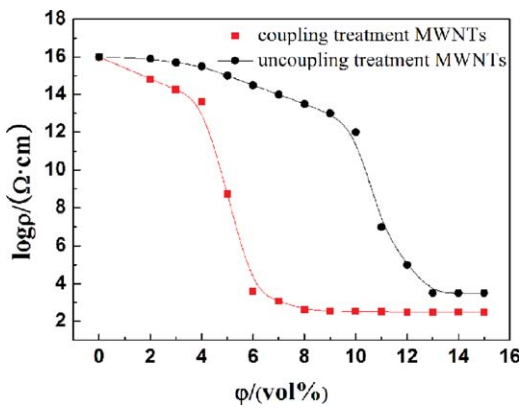

Figure 8. dc conductivity of the MWNT/PA6 composites at room temperature. [Color figure can be viewed in the online issue, which is available at wileyonlinelibrary.com.]

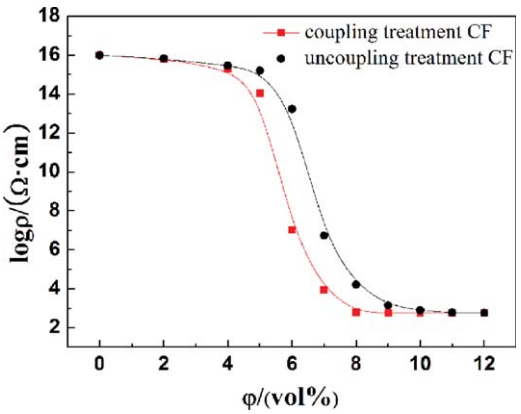

Figure 9. dc conductivity of the CF/PA6 composites at room temperature. [Color figure can be viewed in the online issue, which is available at wileyonlinelibrary.com.]

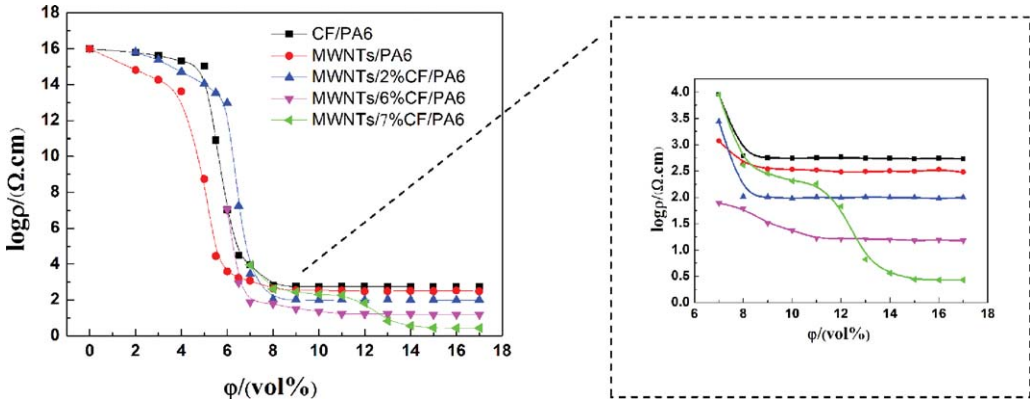

Figure 10. dc conductivity of the MWNT/CF/PA6 composites at room temperature. [Color figure can be viewed in the online issue, which is available at wileyonlinelibrary.com.]

contents. It was clear that the σ values of these MWNT/PA6 composites increased with the rising φ. Meanwhile, the percolation threshold (φ_c) of the KH-550-coupling-treated MWNT composites (4 vol %) was lower than that of the uncoupled MWNT composites (10 vol %). The σ values of the CF/PA6 composite system had the same tendency compared with those of MWNT/PA6 composites, as shown in Figure 9. The φ_c was reduced from 6% for the uncoupled CF/PA6 composites to 5% for the coupling-treated CF/PA6 composites. The functionalized MWNTs and CFs prepared by acidification and amination treatment contained many —COOH and —NH_2 groups on their surface, and these surface molecular groups could create —CONH— bonds between the fillers and the matrix.[35] Thus, this improved both the σ values and the filler dispersion in the composites.

However, the highest σ values of the MWNT/PA6 and CF/PA6 composites were far lower than expected. We found it hard to meet the demands for σ by raising the single-filler content because of the increased filler aggregation. Therefore, to further improve the σ of polymer composites containing nanoscale MWNTs and micrometer-order-sized CFs, three points of concentration ($\varphi_{CF} = 2$, 6, and 7%) from the platform area, percolation area, and stabilization area of the conductive percolation system for the CF/PA6 composite system were chosen. Then, the σ values of the MWNT/CF hybrid fillers in the PA6 matrix were comprehensively analyzed.

As shown in Figure 10, when the volume fraction of the fillers was above 7.5%, the volume resistivity of the MWNT/2% CF/PA6 composites was slightly lower than that of the CF/PA6 and MWNT/PA6 composite systems; this suggested a weak synergistic effect for the MWNT/CF hybrid-filler system. The φ_c of MWNT/2% CF/PA6 composites was 6%; this was greater than that of the CF/PA6 and MWNT/PA6 composite systems. Although the percolation curves for MWNT/PA6 and MWNT/2% CF/PA6 changed sharply in the platform area and had the same φ threshold at 4%, the lower volume resistivity of MWNT/2% CF/PA6 indicated that there was a synergistic impact of the MWNT/2% CF hybrid-filler system.

The volume resistivity reduction of the MWNT/6% CF/PA6 composite system was greater than that of 6% CF/PA6 and the other volume fractions of the CF/PA6 composite system. Furthermore, with the increase in φ, the reduction in the tendency of the volume resistivity in the MWNT/6% CF/PA6 composite system dropped more than that in the CF/PA6 system. The MWNT/6% CF/PA6 composite system had a higher σ compared with the MWNT/PA6 and MWNT/2% CF/PA6 composite systems. All of this hinted that the MWNT/6% CF hybrid-filler system had a better synergistic effect than MWNT/2% CF in PA6.

The percolation curve exhibited a different trend when the same volume fraction of carbon fiber (φ_{CF}) or φ was added to the

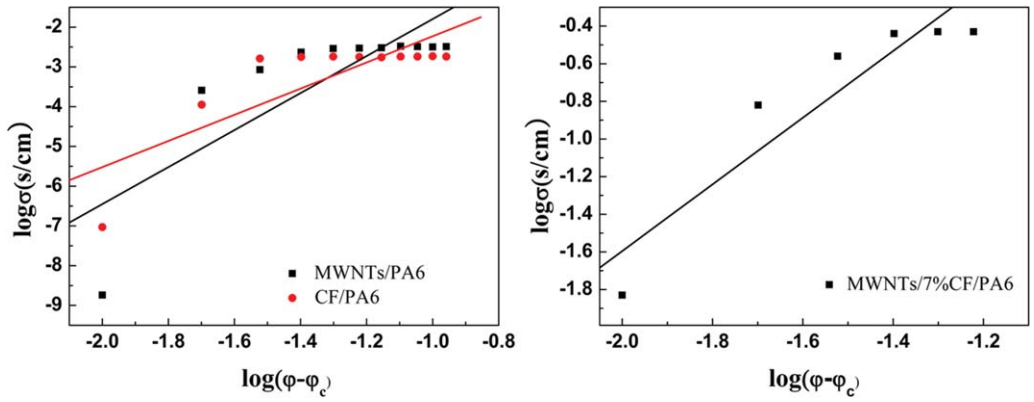

Figure 11. Plots of log σ (S/cm) versus log($\varphi - \varphi_c$) for different types of PA6 composites. [Color figure can be viewed in the online issue, which is available at wileyonlinelibrary.com.]

Table I. φ_c, Critical Exponent, and Relevance Values of the Different Types of PA6 Composites

Type	φ_c	t	Relevancy
MWNT/PA6	4%	4.65	0.81063
CF/PA6	5%	3.29	0.81601
MWNT/7% CF/PA6	11% (4% MWNTs + 7% CF)	1.77	0.92833

7% CF/PA6 composite system, as shown in Figure 10. On the one hand, the volume resistivity of the 7% CF/PA6 composite system did not decrease with the addition of φ_{CF}. On the other hand, with the addition of more MWNTs into the 7% CF/PA6 composites system, the volume resistivity of the 7% CF/PA6 composites system showed a percolation phenomenon again when the hybrid-filler volume content was 11% ($\varphi = 7\%$ CF+4%MWNTs); this was known as the second percolation. The second percolation caused a reduction of two orders of magnitude in the volume resistivity compared with the MWNT/PA6 system; this indicated that the MWNTs effectively improved the σ of the 7% CF/PA6 composite system. Furthermore, as shown in Figure 10, the MWNT/7% CF/PA6 composite system had a better σ than that of MWNT/PA6 composite system before the second percolation. This revealed that there was a synergistic effect between the different fillers. In addition, the second percolation resulted in a reduction the volume resistivity of the composite system only to a small extent compared with the percolation system of CF/PA6 system (named the first percolation). The electron conductivity of the auxiliary conductive path of the MWNTs was weaker than that thorough the conductive framework of the CFs in the polymer matrix.

The conduction of the fillers, the difficulty of forming a conductive network, and the compatibility between the fillers and matrix were the main factors determining the σ values of the polymer composites. An effective conductive network is closely related to the distribution of the fillers; the more uniform the distribution of the fillers is, the more easily an effectively conductive network can be formed at low filler contents. Kirkpatrick's[39] classical statistical percolation could be used to analyze the structure of the conductive network in the MWNT/polymer matrix. The conductive particles could be taken as lattice random distribution points in the polymer matrix, and so, the conductivity of the composite could be expressed as the following law when the fillers content was above φ_c:[40,41]

$$\sigma = \sigma_0(\varphi - \varphi_c)^t \quad (2)$$

where σ is the composite electrical conductivity, σ_0 is an adjustable parameter,[42] and t is a critical exponent. Through the magnitude of t, one can judge the dimensionality of the network in the matrix, and a theoretical value of the exponent between 1.6 and 2.0 indicates a 3D network.[43,44] The closer t is close to this range, the more the filler in the composite system is close to ideal 3D distributions.

Figure 11 presents the relationship between log σ and log($\varphi - \varphi_c$) of the CF/PA6, MWNT/PA6, and MWNT/7% CF/PA6 composite systems. The critical exponents of the single-filler system were 4.65 and 3.29, respectively, for MWNT/PA6 and CF/PA6. They were higher than the predicted universal value; this indicated that percolation took place in the networks with a decrease in the number of dead ends.[45] Compared with the single-filler system, the critical exponent of the MWNT/7% CF/PA6 composite was found to be 1.77; this was closer to the predicted universal value, as shown in Table I. This demonstrated that the hybrid filler of MWNT/CF resulted in scattering closest to a 3D distribution and that the CFs were beneficial to the enhancement of the dispersion of the MWNTs. It also revealed that the nanoscale MWNTs could be dispersed in the framework of the CFs because of the different structures and sizes between the MWNTs and CF.

The electron-transport ability of the filler particles and the 3D electron conductive framework were the key factors determining the value of σ of the polymer composites. As illustrated in Figure 12, the MWNTs and CFs with different sturctures and aspect ratios constituted a more efficient 3D percolating network for electron transport; this resulted in higher σ values of the hybrid-filler composites than those in the single-filler composite. In this study, the MWNTs distributed in the gap of the main truss of the conductive framework was comprised of CFs (Figures 6 and 7). The scheme of the electrically conductive network for the MWNT/CF/PA6 composites is shown in Figure 12(a). The network of the hybrid-filler system was composed of MWNT/PA6 and CF/PA6, so it could be inferred that the CF-to-CF and MWNT-to-MWNT networks of the single-filler

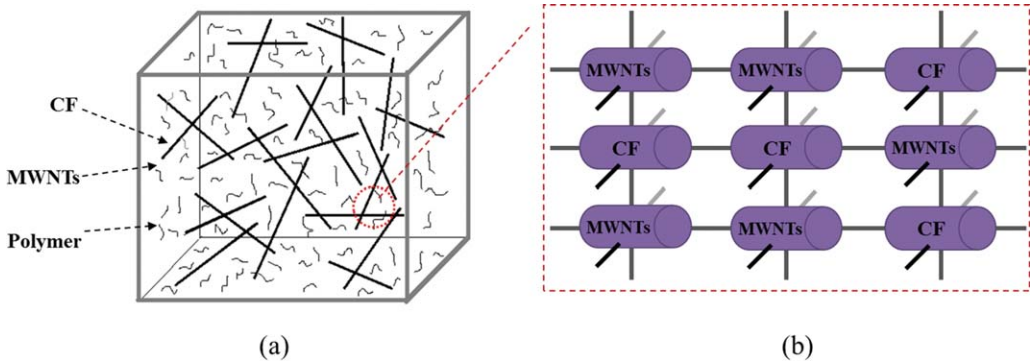

Figure 12. Schematic of the σ network in a PA6 matrix containing a hybrid MWNT/CF filler. [Color figure can be viewed in the online issue, which is available at wileyonlinelibrary.com.]

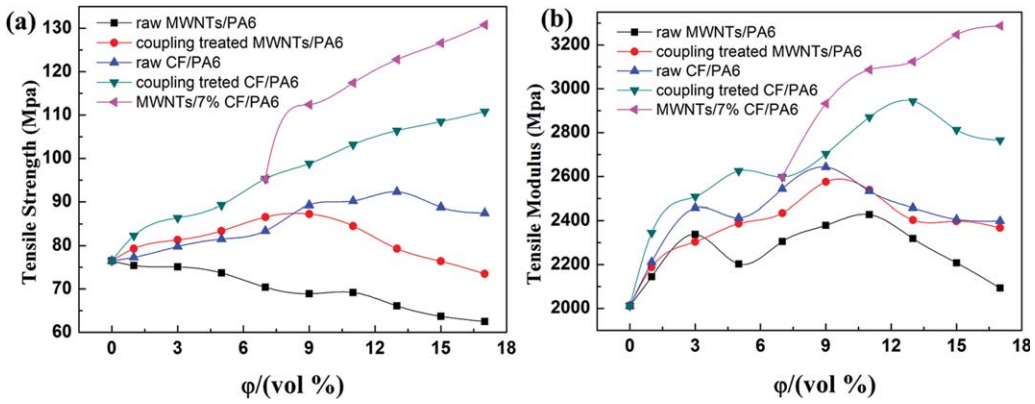

Figure 13. Universal tensile testing: (a) tensile strength and (b) tensile modulus values for the pure PA6 and PA6 composites with different types of fillers. [Color figure can be viewed in the online issue, which is available at wileyonlinelibrary.com.]

systems combined well to produce some effective connections in the hybrid-filler system, as shown in Figure 12(b).

As shown by a synergy conductive value comparison of MWNT/2% CF/PA6, MWNT/6% CF/PA6, and MWNT/7% CF/PA6 composite systems, the MWNTs became a perfect auxiliary conductive network before the formation of the main conductive framework of the CFs. In addition, the unique electrical properties of the MWNTs also enhanced the conductivity of the hybrid-filler system. Primarily, the field emission of the MWNTs caused free electron transfer by the tunnel effect. Moreover, the MWNTs provide free charges in the surroundings because of its specific surface area and low surface energy. When the field energy of the electrons on the CF surfaces was Φ (ev) $\geq$ $|\mu F|$, Φ is the energy of carrier, μ is the migration rate and F is the Faraday constant, the free electrons on CFs were attracted by neighboring MWNT particles and then flowed to the MWNTs. Therefore, the MWNTs were like a conductive bridge dispersed among the framework of the CFs for electron flow inside of the polymer composites.

Mechanical Properties

To investigate the synergetic effect of the hybrid-filler system for other potential applications, the tensile properties for the PA6 composites were investigated. Figure 13 shows the results of the uniaxial tensile testing of the pure PA6 and composites, including the tensile strength and modulus. In both the MWNT/PA6 and CF/PA6 composites, the KH-550-treated single-filler systems had better mechanical properties than the raw single-filler system; this was due to the improved compatibility and dispersion of the fillers by the coupling treatment. The MWNT/7% CF/PA6 composites showed an obvious increase in the tensile properties compared to the PA6 composites with single MWNTs or CFs. The greater tensile properties of the hybrid-filler polymer composites demonstrated that the nanoscale MWNT and micrometer-sized CF hybrid-filler systems had some synergetic effects in improving the mechanical properties. Two factors were suggested to explain the synergetic enhancement of hybrid-filler system composites: (1) the fillers in the hybrid-filler system scattered more homogeneously than the single-filler system; this was caused by the rigid MWNT constructing CFs to form a 3D hybrid structure through the inhibition of further aggregation of the CFs, and (2) fine interfacial bonding between the fillers and matrix was able to efficiently transmit stress form the matrix to the fillers. The KH-550-coupling-treated fillers formed a highly a crosslinked integrated 3D structure; consequently, the mechanical properties of the MWNT/7% CF/PA6 composites increased.

CONCLUSIONS

In this study, a strategy was designed to improve the σ values of PA6 composites through the combination of nanoscale MWNTs and micrometer-sized CF hybrid fillers. A remarkable synergetic effect was shown between the MWNTs and CFs in the enhanced σ values of the PA6 composites. To obtain a good dispersion among fillers and an increase in the matrix–filler interfacial interaction, we modified the surface of the MWNTs and CFs with a silane coupler (KH-550). Chemical surface functionalization increased the σ values of the PA6 composites. The conductivity of the composite system was further improved by the addition of MWNTs to the CF/PA6 composite system. A second percolation appeared in the hybrid-filler system when $\varphi_{CF} \geq 7\%$, and the critical exponent of the MWNT/7% CF/PA6 composites was 1.77. This indicated that the hybrid filler had a good dispersion and scattered close to a 3D network. The mechanical properties of different types of PA6 composites with variation of filler volume content have also been studied. Mechanical analysis results confirmed the synergetic effect of a hybrid-filler system that increased the tensile properties of the composites.

REFERENCES

1. Yang, Y.; Yang, Q.; Li, G. X.; Zhang, P. *Polym. Eng. Sci.* **2007**, *47*, 95.
2. Huang, R. Z.; Xu, X. W.; Lee, S.; Zhang, Y.; Kim, B. J.; Wu, Q. L. *Materials* **2013**, *6*, 4122.
3. Nurdina, A. K.; Maniatu, M.; Samayamuthiran, P. J. *Appl. Polym. Sci.* **2010**, *120*, 857.
4. Sharma, S. P.; Lakkad, S. C. *Compos. A* **2011**, *42*, 8.
5. Azizi, H.; Faghihi, J. *Polym. Compos.* **2009**, *30*, 1743.
6. Yu, A. P.; Ramesh, P.; Sun, X. B.; Bekyarova, E.; Itkis, M. E.; Haddon, R. C. *Adv. Mater.* **2008**, *20*, 4740.

7. Teng, C. C.; Ma, C. C. M.; Chiou, K. C.; Lee, T. M. *Compos. B* **2012**, *43*, 265.
8. Yang, S. Y.; Lin, W. N.; Huang, Y. L.; Tien, H. W.; Wang, J. Y.; Chen, C. C. M.; Li, S. M.; Wang, Y. S. *Carbon* **2011**, *49*, 793.
9. Zhou, T.; Wang, X.; Liu, X. H.; Xiong, D. S. *Carbon* **2010**, *48*, 1676.
10. Yang, K.; Gu, M. Y. *Compos. A* **2010**, *41*, 215.
11. Sumfleth, J.; Adroher, X. C.; Schulte, K. J. *Mater. Sci.* **2009**, *44*, 3241.
12. Ma, P. C.; Liu, M. Y.; Zhang, H.; Wang, S. Q.; Wang, R.; Wang, K.; Wong, Y. K.; Tang, B. Z.; Hong, S. H.; Paik, K. W.; Kim, J. K. *Appl. Mater. Interfaces* **2009**, *1*, 1090.
13. Park, D. H.; Lee, Y. K.; Park, S. S.; Lee, C. S.; Kim, S. H.; Kim, W. N. *Macromolecules* **2013**, *21*, 905.
14. Szentes, A.; Varga, C.; Horváth, G.; Bartha, L.; Kónya, Z.; Haspel, H.; Szél, J.; Kukovecz, Á. *Express Polym. Lett.* **2012**, *6*, 494.
15. Lonjon, A.; Demot, P.; Dantras, E.; Lacabanne, C. J. *Non-Cryst. Solids* **2012**, *358*, 1859.
16. Drubetski, M.; Siegmann, A.; Narkis, M. *Polym. Compos.* **2005**, *26*, 454.
17. Coleman, J. N.; Khan, U.; Blau, W. J.; Gun'ko, Y. K. *Carbon* **2006**, *44*, 1624.
18. Wang, S.; Liang, R.; Wang, B. *Carbon* **2009**, *47*, 53.
19. Lau, K. T.; Hui, D. *Carbon* **2002**, *40*, 1605.
20. Yuen, S. M.; Ma, C. C. M.; Chiang, C. L.; Teng, C. C. *J. Nanomater.* **2008**, *1*, 2008.
21. Li, Y. M.; Recio, L. F.; Gerstel, P.; Srot, V.; Vanaken, P. A.; Kaiser, G.; Burghard, M.; Bill, J. *Chem. Mater.* **2008**, *20*, 5593.
22. Qiu, L.; Chen, Y. K.; Yang, Y. Z.; Xu, L. H.; Liu, X. G. *J. Nanomater.* **2013**, *1*, 2013.
23. Ma, P. C.; Siddiqui, N. A.; Marom, G.; Kim, J. K. *Compos. A* **2010**, *41*, 1345.
24. Yang, D. D.; Xu, H. P.; Wang, J. R.; Wu, Y. H. *J. Appl. Polym. Sci.* **2013**, *130*, 3746.
25. Louis, M.; Joshi, S. P.; Brockmann, W. *Compos. Sci. Technol.* **2001**, *61*, 911.
26. He, X. D.; Zhang, F. H.; Wang, R. G.; Liu, W. B. *Carbon* **2007**, *45*, 2559.
27. Sharma, S. P.; Lakkad, S. C. *Compos. A* **2011**, *42*, 8.
28. Eswaraiah, V.; Aravind, S. S. J.; Ramaprabhu, S. *J. Mater. Chem.* **2011**, *21*, 6800.
29. Vinayan, B. P.; Nagar, R.; Sethupathi, K.; Ramaprabhu, S. *J. Phys. Chem. C* **2011**, *115*, 15679.
30. Kunping, L.; Jingjing, Z.; Guohai, Y.; Guohai, Y.; Chunming, W.; Junjie, Z. *Electrochem. Commun.* **2010**, *12*, 402.
31. Li, L. L.; Liu, K. P.; Yang, G. H.; Wang, C. M.; Zhang, J. R.; Zhu, J. *J. Adv. Funct. Mater.* **2011**, *21*, 869.
32. Ou, J. F.; Wang, J. Q.; Liu, S.; Mu, B.; Ren, J. F.; Wang, H. G.; Yang, S. R. *Langmuir* **2010**, *26*, 15830.
33. Scheibe, B.; Palen, E. B.; Kalenczuk, R. *J. Acta Phys. Polym. A* **2009**, *116*, 150.
34. Jiang, W. L.; Liu, Y.; Wang, J. F.; Wang, Q. T.; Zhang, Y. H.; Guan, S. H. *J. Appl. Polym. Sci.* **2014**, *131*, 1.
35. Qiu, L.; Yang, Y. Z.; Liu, X. G. *Polym. Compos.* **2013**, *34*, 656.
36. Yang, S. Y.; Lin, W. N.; Huang, Y. L.; Tien, H. W.; Wang, J. Y.; Ma, C. C. M.; Li, S. M.; Wang, Y. S. *Carbon* **2011**, *49*, 793.
37. Mahesh, V. H.; Tamanna, R.; Sandrea, B. Y.; Shaik. J. *Compos. Interface* **2010**, *17*, 197.
38. Li, J.; Fang, Z. P.; Tong, L. F.; Gu, A. J.; Liu, F. *J. Appl. Polym. Sci.* **2007**, *106*, 2898.
39. Kirkpatrick, S. *Rev. Mod. Phys.* **1973**, *45*, 574.
40. He, D.; Ekere, N. N. *J. Phys. D: Appl. Phys.* **2004**, *37*, 1848.
41. Lee, M. G.; Nho, Y. C. *Radiat. Phys. Chem.* **2001**, *61*, 75.
42. Guadagno, L.; Vivo, B. D.; Bartolomeo, D.; Lamberti, P.; Sorrentino, A.; Tucci, V.; Vertuccio, L.; Vittoria, V. *Carbon* **2011**, *49*, 1919.
43. Laredo, E.; Prutsky, N.; Bello, A.; Grimau, M.; Castillo, R. V.; Muller, A. J.; Dubois, P. *Eur. Phys. J. E* **2007**, *23*, 295.
44. Adler, J.; Meir, Y.; Aharony, A.; Harris, A. B.; Klein, L. *J. Stat. Phys.* **1990**, *58*, 511.
45. Bhagat, N. A.; Shrivastava, N. K.; Suin, S.; Maiti, S.; Khatua, B. B. *Polym. Compos.* **2013**, *34*, 787.